AIAA 2003-0635

Optimization of Synthetic Jet Actuators

Quentin Gallas, Guiqin Wang, Melih Papila,
Mark Sheplak and Louis Cattafesta

University of Florida
Gainesville, FL

41st Aerospace Sciences
Meeting & Exhibit
6-9 January 2003 / Reno, NV

Report Documentation Page

Form Approved
OMB No. 0704-0188

1. REPORT DATE	2. REPORT TYPE	3. DATES COVERED
JAN 2003		**00-00-2003 to 00-00-2003**

4. TITLE AND SUBTITLE	5a. CONTRACT NUMBER
Optimization of Synthetic Jet Actuators	5b. GRANT NUMBER
	5c. PROGRAM ELEMENT NUMBER
6. AUTHOR(S)	5d. PROJECT NUMBER
	5e. TASK NUMBER
	5f. WORK UNIT NUMBER
7. PERFORMING ORGANIZATION NAME(S) AND ADDRESS(ES) **University of Florida,Department of Electrical and Computer Engineering,Gainesville,FL,32611**	8. PERFORMING ORGANIZATION REPORT NUMBER
9. SPONSORING/MONITORING AGENCY NAME(S) AND ADDRESS(ES)	10. SPONSOR/MONITOR'S ACRONYM(S)
	11. SPONSOR/MONITOR'S REPORT NUMBER(S)

12. DISTRIBUTION/AVAILABILITY STATEMENT
Approved for public release; distribution unlimited

13. SUPPLEMENTARY NOTES
The original document contains color images.

14. ABSTRACT

15. SUBJECT TERMS

16. SECURITY CLASSIFICATION OF:			17. LIMITATION OF ABSTRACT	18. NUMBER OF PAGES	19a. NAME OF RESPONSIBLE PERSON
a. REPORT **unclassified**	b. ABSTRACT **unclassified**	c. THIS PAGE **unclassified**		**11**	

Optimization of Synthetic Jet Actuators

Quentin Gallas,[£] Guiqin Wang,[†] Melih Papila,[¥] Mark Sheplak,[§] and Louis Cattafesta[¶]

Department of Mechanical and Aerospace Engineering
University of Florida
Gainesville, Florida 32611-6250
(352) 846-3017, (352) 392-7303 (FAX), catman@mae.ufl.edu

Abstract

This paper describes the optimization of a piezoelectric-driven synthetic jet actuator based on a Lumped Element Modeling (LEM). To simplify the problem, this papers splits the optimization problem into two parts. First, a constrained optimization of the cavity volume and orifice dimensions of two baseline synthetic jets, each with a given piezoelectric diaphragm, is conducted using two different objective functions. One seeks to improve the centerline output velocity over a broad frequency range, and the other maximizes the centerline velocity at a prescribed resonant frequency of the device. Significant improvements are achieved using both objective functions for both synthetic jets. Second, the two baseline piezoelectric diaphragms have been optimized using two configurations. One uses the standard inner-disc piezoceramic patch bonded to a metal shim, while the other employs an outer piezoceramic ring. In each case, the objective is to maximize the achievable volume displacement of the diaphragm at the coercive electric field strength of the piezoceramic, while the natural frequency of the piezoelectric diaphragm is constrained to be greater than or equal to the baseline designs. Both configurations yield modest (~5%) improvements for one diaphragm and significant improvements for the other diaphragm (>50%).

Nomenclature

a_0 orifice radius (mm)

c_0 air speed of sound (m/s)

C_{aC} cavity acoustic compliance = $V_0/\rho_0 c_0^2$ ($s^2 \cdot m^4/kg$)

C_{aD} diaphragm short-circuit acoustic compliance = $\Delta V/P\big|_{V_{ac}=0}$ ($s^2 \cdot m^4/kg$)

C_{EF} piezoceramic electrical free capacitance (F)

d_a effective acoustic piezoelectric coefficient = $\Delta V/V_{ac}\big|_{P=0}$ (m^3/V)

$E_{f\max}$ maximum electric field (V /m)

f frequency (Hz)

f_H Helmholtz frequency = $1/2\pi\sqrt{(M_{aN}+M_{aRad})C_{aC}}$ (Hz)

f_D short-circuit diaphragm resonant frequency = $1/2\pi\sqrt{M_{aD}C_{aC}}$ (Hz)

f_1, f_2 synthetic jet lowest and highest resonant frequencies, respectively (Hz)

K_D nondimensional orifice jet dump loss coefficient

L orifice length (mm)

M_{aD} diaphragm acoustic mass (kg/m^4) = $\frac{2\pi}{\Delta V^2}\int_0^{R_2}\rho_A\left[w(r)\right]^2 r\,dr$

M_{aN} orifice acoustic mass (kg/m^4) = $4\rho_0 L/3\pi a_0^2$ for Poiseuille flow

M_{aRad} orifice acoustic radiation mass = $8\rho_0/3\pi^2 a_0$ (kg/m^4)

P differential pressure on the diaphragm (N/m^2)

q electric charge stored on the piezoelectric (C)

Q_c volume flow rate through the cavity (m^3/s)

Q_{out} volume flow rate through the orifice (m^3/s)

Q volume flow rate displaced by the diaphragm = $Q_c + Q_{out}$ (m^3/s)

R_{aD} diaphragm acoustic resistance = $2\zeta\sqrt{M_{aD}/C_{aD}}$ ($kg/s \cdot m^4$)

R_{aN} viscous orifice acoustic resistance ($kg/s \cdot m^4$) = $8\nu\rho_0 L/\pi a_0^4$ for Poiseuille flow

R_{aO} nonlinear orifice acoustic resistance = $0.5K_D\rho_0 Q_{out}/\pi^2 a_0^4$ ($kg/s \cdot m^4$)

R_1 piezoceramic radius (mm)

[£] Graduate Student, Student Member AIAA.

[†] Graduate Student.

[¥] Post Doctoral Research Associate, Member AIAA.

[§] Assistant Professor, Member AIAA.

[¶] Assistant Professor, Associate Fellow, AIAA.

R_2 shim radius (mm)

s Laplace variable = $j\omega$

t_p piezoceramic thickness (mm)

t_s shim thickness (mm)

u_0 centerline orifice velocity (m/s)

V_{ac} input ac voltage (V)

$V_{ac,\max}$ maximum applied voltage = $t_p \times E_{f\max}$ (V)

V_0 cavity volume (mm^3)

$w(r)$ transverse displacement of the diaphragm (m)

ΔV volume displaced by the diaphragm = $\int_0^{R_2} 2\pi r w(r)\, dr$ (m^3)

ϕ_a electroacoustic turns ratio of the piezoceramic diaphragm = $\left| d_a / C_{aD} \right|$ (Pa/ V)

ν air kinematic viscosity (m^2/s)

ρ_A area density (kg/m^2)

ρ_0 air density (kg/m^3)

ω radian frequency = $2\pi f$ (rad/s)

ζ empirical diaphragm damping coefficient

Introduction

Synthetic or "zero-net mass flux" jets[1] are commonly used as flow-control actuators in a wide spectrum of applications including jet vectoring,[2] separation control,[3,4] and boundary layer control.[5,6] The performance specifications of any actuator are quantified in terms of an exhaustive list of parameters such as bandwidth, control authority, etc. Flow-control applications require a known actuator frequency response function that relates the input voltage to the output property of interest (e.g., maximum velocity, volumetric flow rate, momentum flux, etc.). Clearly, the required performance metrics are application specific, and methods are needed to achieve the optimal design of these devices. Design and optimization studies have been conducted for piezoelectric cantilever-type flow control actuators, but the modeling issues are simpler compared to synthetic jets.[7] Specifically, the cavity and orifice configuration of a synthetic jet significantly complicates the overall system dynamics. Recently, LEM has been combined with equivalent circuit representations to estimate the nonlinear dynamic response of a synthetic jet as a function of device dimensions and material properties.[8,9] These models have provided good agreement between predicted and measured frequency response functions and thus are suitable for use as design tools.

The purpose of this paper is to leverage LEM in the optimization of piezoelectric-driven synthetic jet actuators. The following section briefly reviews the lumped element model and corresponding equivalent circuit of a synthetic jet from Gallas et al.[8] and discusses the basic dynamic behavior. The resulting system model is then employed in an optimization scheme. For the current study, the optimization problem is decoupled into two parts. First, the piezoelectric diaphragm is fixed while the cavity volume and orifice dimensions are varied. Second, the piezoelectric diaphragm is optimized while the other design parameters are fixed. Discussions on the chosen cost functions and accompanying constraints employed in the optimization and the corresponding results are presented. This paper is concluded with a discussion of the results and future work.

Design Problem and Analysis

In this section, the lumped element model of a piezoelectric-driven synthetic jet is reviewed and the basic dynamic behavior discussed.

Lumped Element Model

At low frequencies, where the characteristic length scales of the governing physical phenomena are much larger than the largest geometric dimension, the governing partial differential equations of the dynamic system can be "lumped" into a set of coupled ordinary differential equations.[10] The resulting lumped-parameter system can then be represented as an equivalent electrical circuit possessing idealized discrete circuit elements and conjugate power variables for the equivalent voltage and current.[11] This approach provides a simple method to estimate the non-linear dynamic response of a synthetic jet actuator for design and optimization purposes.

A cross-sectional schematic and corresponding equivalent circuit representation for a typical piezoelectric-driven synthetic jet are shown in Figure 1. The details of the circuit parameter estimation techniques, assumptions, and limitations are given by Gallas et al.[8] The structure of the equivalent circuit is explained as follows. A harmonic voltage V_{ac} is applied across the piezoceramic to create an effective acoustic pressure that drives the diaphragm into motion. This represents a conversion from electrical energy to acoustic energy and is represented by an ideal transformer possessing a turns ratio ϕ_a. The motion of the diaphragm (i.e., volume velocity, Q) can store potential energy via compressibility effects in the cavity (Q_c) and/or can store kinetic energy via oscillatory flow through the orifice (Q_{out}). Physically, this is represented as a volume velocity divider, $Q = Q_c + Q_{out}$.

There are several simplifying assumptions employed in the current model. First, the synthetic jet is assumed to exhaust into a semi-infinite quiescent air medium. In practice, these devices interact with a boundary layer that greatly alters the jet-exit velocity profile and thus the total orifice impedance.[12] The corresponding differences in the frequency response functions of a synthetic jet actuator exhausting into a quiescent medium versus one exhausting into a boundary layer means that the bench-top calibration of these devices is insufficient to accurately estimate the volume velocity or momentum flux exhausted into a cross flow for a given excitation voltage. Second, compressibility effects in the orifice, but not in the cavity, are neglected. The incorporation of these effects into the lumped element model is an ongoing research area both in the flow control actuator community as well as the engine nacelle acoustic liner community.[13]

Equivalent Circuit Model

Before conducting a formal optimization, the basic dynamic features of the system are reviewed. The frequency response function of the volume flow rate through the orifice per applied voltage for the equivalent circuit shown in Figure 1 is a four-pole, single-zero dynamic system,[8]

$$\frac{Q_{out}(s)}{V_{ac}(s)} = \frac{d_a s}{a_4 s^4 + a_3 s^3 + a_2 s^2 + a_1 s + 1}, \qquad \{1\}$$

where

$$\begin{aligned} a_1 &= C_{aD}\left(R_{aO} + R_{aN} + R_{aD}\right) \\ &\quad + C_{aC}\left(R_{aO} + R_{aN}\right), \\ a_2 &= C_{aD}\left(M_{aRad} + M_{aN} + M_{aD}\right) \\ &\quad + C_{aC}\left(M_{aRad} + M_{aN}\right) + C_{aC}C_{aD}R_{aD}\left(R_{aO} + R_{aN}\right), \qquad \{2\} \\ a_3 &= C_{aC}C_{aD}\begin{bmatrix} M_{aD}\left(R_{aO} + R_{aN}\right) \\ + \left(M_{aRad} + M_{aN}\right)R_{aD} \end{bmatrix}, \text{ and} \\ a_4 &= C_{aC}C_{aD}M_{aD}\left(M_{aRad} + M_{aN}\right). \end{aligned}$$

To first order, the coefficients in Eq. {2} are constants determined via simple algebraic expressions as a function of geometry and material properties. This model includes one empirical constant, R_{aD}, that represents the structural damping of the piezoelectric composite. In general, some of the coefficients exhibit frequency and amplitude dependence (i.e., due to nonlinear effects). Specifically, R_{aO} is a non-linear orifice resistance that is proportional to the volume velocity, $Q_{out}(s)$.

For a dc voltage ($s = 0$), the volume velocity is zero. At low frequencies ($s \to 0$), the volume velocity is proportional to $j\omega d_a V_{ac}$. At high frequencies ($s \to \infty$),

$$\frac{Q_{out}}{V_{ac}} \cong \frac{d_a}{C_{aC}C_{aD}M_{aD}\left(M_{aN} + M_{aRad}\right)s^3}, \qquad \{3\}$$

and the output attenuates at 60 dB/decade.

The four-pole system in Eq. {1} possesses two resonant frequencies, f_1 and $f_2 > f_1$, that are related to the short-circuit piezoelectric diaphragm natural frequency f_D,

$$f_D = \frac{1}{2\pi}\sqrt{\frac{1}{M_{aD}C_{aD}}}, \qquad \{4\}$$

and the Helmholtz resonator frequency f_H,

$$f_H = \frac{1}{2\pi}\sqrt{\frac{1}{\left(M_{aN} + M_{aRad}\right)C_{aC}}}, \qquad \{5\}$$

by the equality

$$f_1 f_2 = f_D f_H. \qquad \{6\}$$

From Eq. {6}, it is obvious that the cavity volume and the orifice dimensions, as well as the piezoelectric-diaphragm characteristics determine the dynamic response of the synthetic jet.

Model Verification

Gallas et al.[8] have experimentally validated the lumped element model for two different prototypical synthetic jet actuators using phase-locked Laser-Doppler Velocimetry. For illustration purposes, these results are briefly reviewed. The dimensions and properties of the devices are given in Table 1 and Table 2. The amplitude of the piezoelectric excitation voltage was 25 V in all cases. The comparison between the full nonlinear model prediction and the experiments are shown in Figure 2 and Figure 3. In both figures, the centerline velocity magnitude is plotted as a function of frequency. For the lumped element model predictions, the centerline velocity was estimated by modeling the flow in the orifice as flow in a circular duct driven by an oscillatory pressure gradient. The first case (I, Figure 2) clearly illustrates the two resonant frequencies of the coupled oscillator. The second case (II, Figure 3) corresponds to a system possessing a single dominant peak. The lower peak at $f_1 \approx 315$ Hz is heavily damped in this case due to the frequency dependent nonlinear orifice resistance term R_{aO}. In both cases, there is sufficient agreement between prediction and experiment to justify the employment of LEM as a design and optimization tool. It is important to note

that the underlying assumptions used to derive each lumped element limit the applicable frequency range of the corresponding element from dc to some upper limiting frequency (see, for example, Rossi[10]).

Table 1: Piezoceramic diaphragm details.

	Case	
Shim (Brass)	**I**	**II**
Elastic Modulus (Pa)	8.963×10^{10}	
Poisson's Ratio	0.324	
Density (kg/m^3)	8700	
Thickness (mm)	0.20	0.10
Diameter (mm)	23.5	37
Piezoceramic (PZT-5A)		
Elastic Modulus (Pa)	6.3×10^{10}	
Poisson's Ratio	0.33	
Density (kg/m^3)	7700	
Thickness (mm)	0.11	0.12
Diameter (mm)	20.0	25.0
Rel. Dielectric Constant	1750	
d_{31} (m/V)	-1.75×10^{-10}	
C_{EF} (F)	4.42×10^{-8}	6.33×10^{-8}

Table 2: Synthetic jet details.

	Case	
Cavity:	**I**	**II**
Volume V_0 (m^3)	2.50×10^{-6}	5.00×10^{-6}
Orifice:		
Radius a_0 (mm)	0.825	0.42
Length L (mm)	1.65	0.84

Optimization of a Synthetic Jet

The lumped element model presented in the previous section is a powerful design tool that enables the multi-energy domain dynamic modeling of a synthetic jet actuator. In this section, the model is used as a vehicle to enable optimization. For simplicity and physical insight, the optimization problem is decoupled into two parts. First, the piezoelectric diaphragm is held constant, and the cavity volume and orifice dimensions are varied. Two different cost-functions and sets of constraints are explored for this problem. Next, the piezoelectric diaphragm is optimized and various concepts for the driver configuration are presented along with their associated results. In all cases, the optimization problem was solved via MATLAB's optimization toolbox.

Orifice/Cavity Optimization

For a given piezoelectric composite diaphragm, the device behavior is governed by the cavity volume V_0, the orifice radius a_0, and orifice length L. For example, Figure 4-Figure 6 illustrate the effect of varying V_0, a_0, and L on the centerline velocity output of the "nominal" synthetic jet actuator shown in Figure 2 (Case I). Increasing the cavity volume results in a larger acoustic compliance, C_{aC}, and thus lowers first resonance, $f_1 \propto 1/\sqrt{V_0}$, and also decreases the overall broadband amplitude, while slightly reducing the second resonant frequency relative to the nominal case (Figure 4). Increasing the orifice radius decreases total acoustic mass, $M_{aN} + M_{aRad}$, resulting in a higher first resonance and a correspondingly higher second resonance (Figure 5). Conversely, increasing the orifice length increases the total acoustic mass, $M_{aN} + M_{aRad}$, and thus reduces the first resonance, much in the same manner as varying the cavity volume (Figure 6). It is clear that varying these three geometric variables can significantly affect the frequency response function.

Different flow control applications will require different frequency response specifications in terms of bandwidth and the output physical quantity of interest. For example, certain applications may require significant actuation authority in terms of momentum flux over a narrow frequency range, while another may require a flat, broadband response possessing a prescribed minimum centerline velocity. This emphasizes the importance of clearly specifying a design objective.

In addition to choosing a design objective, the optimization problem requires the specification of various constraints. These constraints can be broadly classified into three categories: performance constraints, design variable constraints, and model constraints. Performance constraints may consist of specifying the desired locations of the resonant frequencies, the flatness tolerance of the gain factor of the frequency response function, etc. Design variable constraints may be needed due to physical limitations based on manufacturability, packaging considerations, material failure, etc. As stated at the end of the previous section, there are limits to the applicability of each lumped element as a function of frequency. Therefore, after an optimal solution is achieved, the validity of the assumptions in the model must be evaluated, or the optimization problem must be constrained by the limitations of the model. The latter approach was chosen for this study. For example, the lumped elements for the piezoelectric composite are limited to frequencies below the second natural frequency of the composite diaphragm. The size of the cavity is limited such that the impedance of the cavity can be approximated by a compliance.[8] Another limitation appears for the orifice aspect ratio, L/a_0. Based on experimental results for several cases, Gallas[9] found that

reasonable agreement was achieved between the lumped element model and measured dynamic response when the orifice aspect ratio approximately exceeded unity.

For the present optimization study, the goal is to improve the performance of the nominal designs presented in Figure 2 (Case I) and Figure 3 (Case II). The objective function, constraints, and design variables are summarized in Table 3. Specifically, Case I is optimized using one cost function, while Case II is optimized using two different cost functions.

The first cost function employed maximizes the integrated centerline velocity over the entire frequency range, $\int_0^{f_{\lim}} u_0(f)\,df$ where the upper limit of integration is 3000 Hz and 1500 Hz for Case I and II, respectively. The motivation for such an objective function is to increase the broadband response of the actuator. The constraints on the orifice radius are motivated by device manufacturability and flow perturbation concerns, while the minimum orifice length constraint is driven by the requirement that the orifice plate be rigid. The volume range is dictated by size limitations. In addition, constraints are imposed on the orifice aspect ratio and by fixing the piezoelectric drive voltage. Figure 7 shows the resulting optimized frequency response function compared to the nominal response for Case I. The frequency response function increased over the entire frequency range by decreasing V_0, a_0, and L. In addition, the first resonant peak is heavily damped in the optimized response.

The results using a similar approach for Case II are shown in Figure 8. Again, the frequency response function increased over nearly the entire frequency range by decreasing V_0, a_0, and L. In addition, the flat portion of the response function is increased and the second resonant peak is moved to a higher frequency. This actuator design is useful for applications that require a flat broadband response.

The second cost function employed maximizes the centerline velocity at the second resonant frequency of the system, $u_0(f_2)$. From a practical standpoint, this optimization is useful for applications requiring high actuation authority over a narrow frequency range. The constraints on the orifice and cavity geometry, as well as the aspect ratio and drive voltage are similar to those outlined above. A new equality constraint, however, is placed on the location of the second resonant frequency. The results of this optimization for Case II are shown in Figure 9. The second resonant peak is increased as desired (by ~ 35%). In addition, the broadband response, especially at the lower frequencies, is increased with respect to the nominal case.

While the optimization studies in this section indicate the promise of improved performance, additional gains can likely be achieved by optimizing the piezoelectric composite diaphragm. This is described in the next section.

Table 3: Summary of optimization problem for a synthetic jet actuator.

Objective	Constraints	Variables
$\int_0^{f_{\lim}} u_0(f)\,df$	• Upper/Lower bounds on variables: Case I: $\begin{cases} 0.125 \le a_0 \le 2 \\ 0.5 \le L \le 20 \\ 1152 \le V_0 \le 47,640 \end{cases}$ Case II: $\begin{cases} 0.125 \le a_0 \le 2 \\ 0.38 \le L \le 20 \\ 780 \le V_0 \le 21,270 \end{cases}$ • Orifice aspect ratio $L/a_0 \ge 1$ • Fixed input voltage V_{ac} = 25 V	a_0 L V_0
$u_0(f_2)$	• Upper/Lower bounds on variables: Case II: $\begin{cases} 0.125 \le a_0 \le 2 \\ 0.38 \le L \le 20 \\ 780 \le V_0 \le 21,270 \end{cases}$ • Natural frequency f_2 = 820 Hz • Orifice aspect ratio $L/a_0 \ge 1$ • Fixed input voltage V_{ac} = 25 V	a_0 L V_0

Piezoelectric Composite Optimization

For a given cavity/orifice configuration, the response of the synthetic jet is directly proportional to the effective acoustic piezoelectric coefficient, d_a, as shown in Eq. {1}. The response is also governed by the natural frequency of the diaphragm, f_D, which is a function of the acoustic mass, M_{aD}, and short-circuit acoustic compliance, C_{aD}, of the piezoelectric diaphragm. These lumped elements are all dictated by the geometry and material properties of the diaphragm.

Before conducting a formal optimization of the piezoelectric composite diaphragm, the basic modeling concepts are reviewed. Top-view and cross-sectional schematics of two axisymmetric piezoelectric composite plate configurations examined in this study are shown in Figure 10-Figure 13. The first type (Figure 10 and Figure 11) consists

of an inner circular disc, possessing a piezoceramic material of thickness t_p and radius R_1 bonded to a shim material of radius R_2 and thickness t_s. The second type (Figure 12 and Figure 13) consists of an annular ring possessing a piezoceramic material of radial extent $R_2 - R_1$ bonded to a shim material of radius R_2. In general, the actuator is subjected to an applied voltage V_{ac} across the piezoceramic thickness. This loading creates both transverse $w(r)$ and radial $u(r)$ displacements.

Ideally, a piezoelectric actuator is a linear, conservative, reciprocal transducer.[10] The piezoelectric composite deforms in response to both an applied ac voltage and a differential pressure. The lumped piezoelectric coupling equations for the transduction model are[14]

$$\begin{Bmatrix} \Delta V \\ q \end{Bmatrix} = \begin{bmatrix} C_{aD} & d_a \\ d_a & C_{EF} \end{bmatrix} \begin{Bmatrix} P \\ V_{ac} \end{Bmatrix}, \qquad \{7\}$$

where ΔV is the volume displaced by the plate due to the application of a differential pressure P and/or voltage V_{ac}, q is the charge stored on the piezoelectric electrodes, C_{EF} is the electrical free capacitance of the piezoelectric material, C_{aD} is the short-circuit acoustic compliance of the plate, and d_a is the effective acoustic piezoelectric coefficient.

The acoustic mass M_{aD} is determined by equating the lumped kinetic energy of the vibrating diaphragm expressed in acoustic conjugate power variables to the total kinetic energy. The determination of the lumped element parameters for this two-port model requires the solution of the transverse static deflection field as a function of pressure and voltage loading. For this study, linear laminated plate theory is used to solve for the transverse static deflection, and an optimization scheme is then implemented using this two-port model. The details of the composite plate model are presented in Prasad et al.[14]

The material properties are E_s, ν_s, E_p, and ν_p, where the subscripts 's' and 'p' denote the shim and piezoelectric, respectively, while E, ν, and d_{31} are the elastic modulus, Poisson's ratio, and piezoelectric constant, respectively. In this study, the material properties are constant and are listed in Table 1.

The optimization objective function maximizes the achievable displaced volume per applied voltage, $d_a = \Delta V\big|_{P=0} / V_{ac,\max}$, compared to the nominal values for Cases I and II. The motivation behind this objective function is that the strength of a piezoelectric-driven synthetic jet is directly proportional to this quantity. Note that $V_{ac,\max}$ is the maximum voltage that can be applied to the piezoelectric without depolarization and is estimated as

$$V_{ac,\max} = t_p \times E_{f\max} \cong t_p \times (30V/mil), \qquad \{8\}$$

where $E_{f\max}$ is the coercive electric field applied through the thickness t_p of the piezoceramic.

Next, constraints are defined. Reasonable lower and upper bounds are defined for the geometric variables t_s, t_p and R_1, while R_2 is fixed in this study. The resonant frequency of the composite diaphragm plays an important role in the design process. Without a constraint, the optimization results in a very compliant diaphragm that can achieve large volume displacements but has a low natural frequency. Since bandwidth is often an important quantity, a lower bound is placed on the resonant frequency of the diaphragm. The goal here is to improve the performance of the diaphragm compared to the existing designs in Table 1. Thus, the fundamental frequencies of the nominal designs used in Cases I and II are chosen as the lower bound.

Optimizations of both the inner-disc and outer-ring configurations were thus performed for Cases I and II using the MATLAB optimization toolbox. The results are summarized in Table 4 for the inner-disc configuration. The optimum design slightly improves (by ~6%) the volume displacement achieved for the nominal Case I, while a 52% improvement is achieved compare to the nominal Case II. It should be noted that the lower frequency bound on f_D is always active in the optimized design, indicating that a direct comparison of d_a between the original and optimized designs is justified.

Table 4: Optimization results of piezoelectric diaphragms with an inner-disc configuration.

	I		**II**	
	Original	**Optimum**	**Original**	**Optimum**
R_2 (mm)	11.5	11.5	18.5	18.5
R_1 (mm)	10.0	10.5	12.5	16.9
t_s (mm)	0.15	0.10	0.10	0.08
t_p (mm)	0.08	0.16	0.11	0.12
f_D (Hz)	**2114**	**2114**	**632**	**632**
d_a (x10^{-10}) (m^3/V)	**0.553**	**0.586**	**4.32**	**6.56**

The optimization results are summarized in Table 5 for the outer-ring configuration. The

performance improvement is 3% and 46% compared to the nominal Case I and II designs, respectively. The performance improvement is less than the inner-disc configuration. However, the outer-ring configuration is less apt to lead wire failures than the inner-disc case due to the reduced motion near the clamp (see Figure 13).

Table 5: Optimization results of piezoelectric diaphragms with an outer-ring configuration.

	I	II
R_2 (mm)	11.5	18.5
R_1 (mm)	7.0	10.9
t_s (mm)	0.13	0.095
t_p (mm)	0.056	0.048
f_D (Hz)	**2114**	**632**
d_a (x10^{-10}) (m^3/V)	**0.568**	**6.30**

Other configurations are possible and will be studied in future work. For example, oppositely-polarized inner- and outer-rings can be combined in both unimorph and bimorph designs.

Conclusions and Future Work

The optimization of a piezoelectric-driven synthetic jet actuator based on LEM has been carried out. It has been shown that LEM is a viable tool to optimally design these devices for candidate applications. To simplify the problem, the current study has split the optimization problem into two parts by separately optimizing the (1) cavity volume and orifice dimensions and (2) the piezoelectric diaphragm.

A constrained optimization of the cavity volume and orifice dimensions of two baseline synthetic jets, each with a given piezoelectric diaphragm, has been conducted using two different objective functions. One function seeks to improve the centerline output velocity, which is a representative measure of the device output, over a broad frequency range of interest. The other objective function focuses on maximizing the centerline velocity at a prescribed resonant frequency of the device. Significant improvements have been achieved for all cases.

In addition, two candidate piezoelectric diaphragm configurations have been optimized. One uses the standard inner-disc piezoceramic patch bonded to a metal shim, while the other uses an outer piezoceramic ring. In each case, the objective is to maximize the achievable volume displacement of the diaphragm, corresponding to the coercive electric field strength of the piezoceramic. The natural frequency of the piezoelectric diaphragm was constrained to be greater than or equal to that of the baseline designs. Both methods yield modest (~5%) improvements for one diaphragm and significant improvements for the other diaphragm (>50%). The inner-disc configuration yields slightly better performance, but is likely to be more susceptible to lead-wire breakage.

In future work, experiments will be conducted to confirm the optimization results presented here. Other piezoceramic diaphragm configurations will be studied. In addition, a coupled constrained optimization will be carried out that seeks to optimize the device performance by simultaneously varying the piezoelectric diaphragm dimensions, cavity volume, and orifice dimensions.

Also, another optimization problem of a synthetic jet will be investigated. The current study is limited to improving an existing baseline design. Perhaps the more interesting case is the optimal design synthesis problem. In this problem, the designer seeks to achieve a desired frequency response function. Due to the nonlinear nature of the system, the design objective can be approximated by a linear transfer function that is valid at a particular driving voltage. A key challenge here is that the end user must be able to translate desirable actuator characteristics into quantitative design goals.

Acknowledgments

The authors gratefully acknowledge grant support from NASA Langley (monitored by S. Gorton) and AFOSR (monitored by Dr. J. Schmisseur).

References

1. Smith, B. L. and Glezer, A., "The Formation and Evolution of Synthetic Jets," Physics of Fluids, Vol. 10, No. 9, pp. 2281-2297, 1998.

2. Smith, B.L. and Glezer, A., "Vectoring and Small-Scale Motions Effected in Free Shear Flows Using Synthetic Jet Actuators," AIAA paper 97-0213, 1997.

3. Crook, A., Sadri, A. M., and Wood, N. J., "The Development and Implementation of Synthetic Jets for the Control of Separated Flow," AIAA Paper 99-3176, July 1999.

4. Amitay, M., Kibens, V., Parekh, D., and Glezer, A., "The Dynamics of Flow Reattachment Over a Thick Airfoil Controlled by Synthetic Jet Actuators," AIAA paper 99-1001, 1999.

5. Rathnasingham, R. and Breuer, K. S., "Coupled Fluid-Structural Characteristics of Actuators for Flow Control," *AIAA Journal*, Vol. 35, No. 5, pp. 832-837, May 1997.

6. Lee, C.Y., and Goldstein, D.B., "DNS of Microjets for Turbulent Boundary Layer Control," AIAA paper 2001-1013, 2001.

7. Cattafesta, L., Garg, S., and Shukla, D., "Development of Piezoelectric Actuators for Active Flow Control," *AIAA Journal*, Vol. 39, No. 8, pp. 1562-1568, August 2001.

8. Gallas, Q., Holman, R., Nishida, T., Carroll, B., Sheplak, M., and Cattafesta, L., "Lumped Element Modeling of Piezoelectric-Driven Synthetic Jet Actuators," *AIAA Journal*, Vol. 41, No 2, January 2003.

9. Gallas, Q., "Lumped Element Modeling of Piezoelectric-Driven Synthetic Jet Actuators for Active Flow Control," M.S. Thesis, Department of Mechanical and Aerospace Engineering, University of Florida, Gainesville, FL, 2002.

10. Rossi, M., Acoustics and Electroacoustics, Artech House, Norwood, MA, pp. 245-373, 1988.

11. Senturia, S. D., Microsystem Design, Kluwer Academic Publishers, 2001.

12. Mittal, R., Rampuggoon, P., Udaykumar, H. S., "Interaction of a Synthetic Jet with a Flat Plate Boundary Layer," AIAA Paper 2001-2773, June 2001.

13. Motsigner, R. E., and Kraft, R. E., "Design and Performance of Duct Acoustic Treatment," in Aeroacoustics of Flight Vehicles: Theory and Practice, Volume 2: Noise Control, edited by Hubbard, H. H., Acoustical Society of America, New York, 1995.

14. Prasad, S., Horowitz, S., Gallas, Q., Sankar, B., Cattafesta, L., and Sheplak, M., "Two-Port Electroacoustic Model of an Axisymmetric Piezoelectric Composite Plate," AIAA Paper 2002-1365, 43rd AIAA/ASME/ASCE/AHS Structures, Structural Dynamics, and Materials Conference, April 2002.

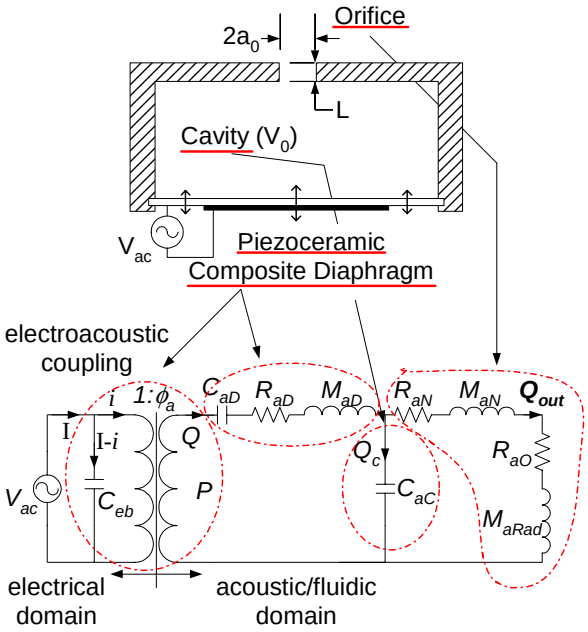

Figure 1: Schematic representation and equivalent circuit model of a piezoelectric-driven synthetic jet.

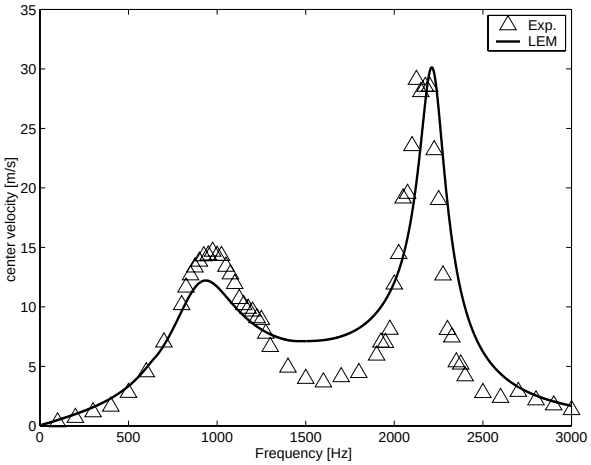

Figure 2: Comparison between the lumped element model and experiment for Case I.[8]

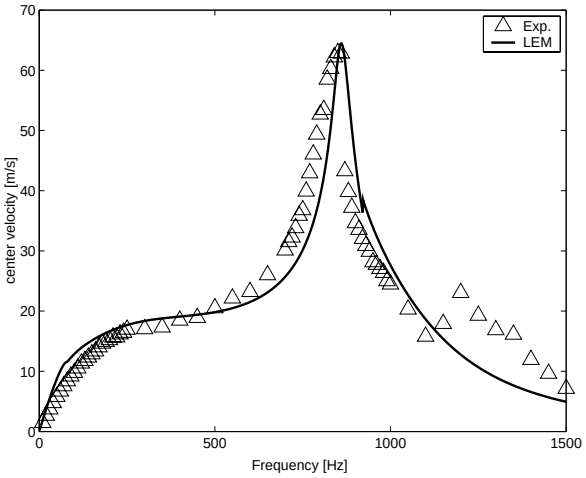

Figure 3: Comparison between the lumped element model and experiment for Case II.[8]

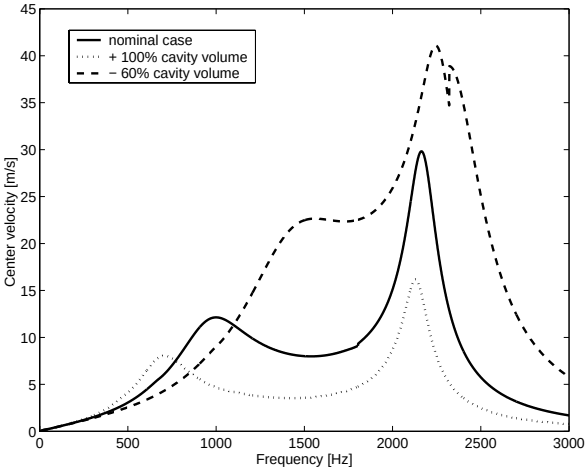

Figure 4: Lumped element model prediction for varying cavity volume (Case I).

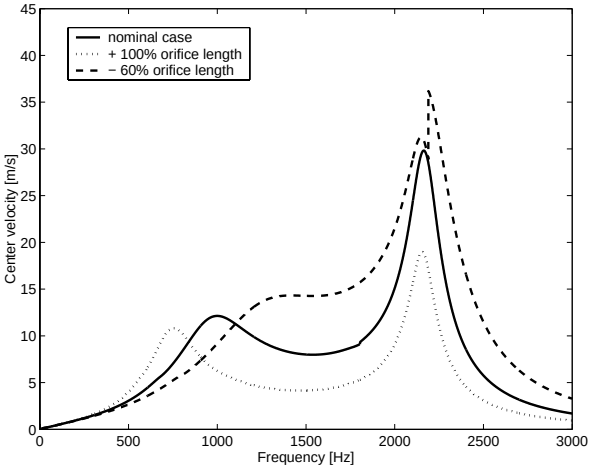

Figure 5: Lumped element model prediction for varying orifice radius (Case I).

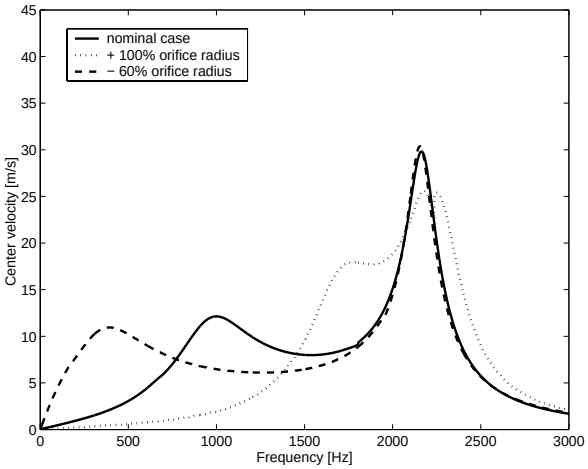

Figure 6: Lumped element model prediction for varying orifice length (Case I).

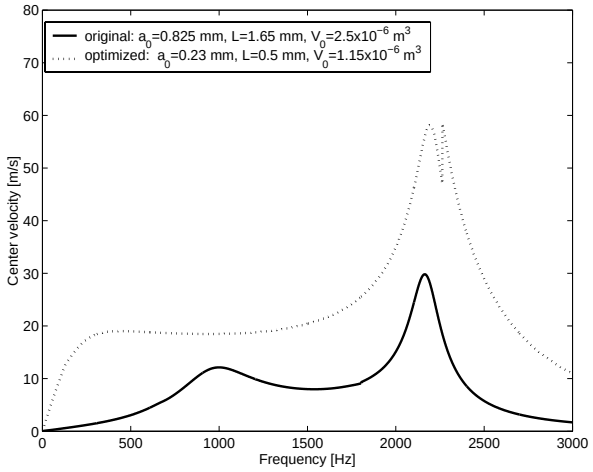

Figure 7: Optimization of Case I, maximizing the overall output.

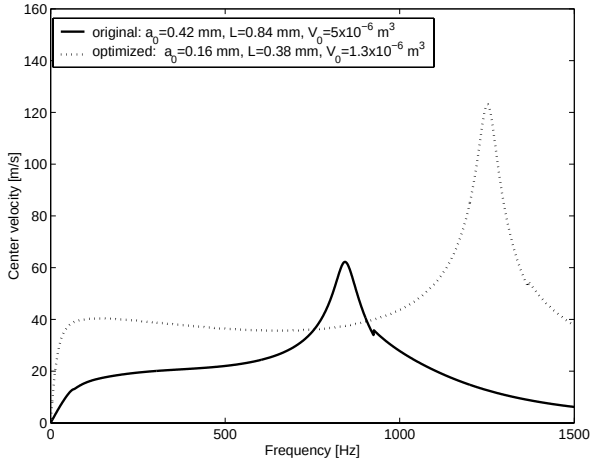

Figure 8: Optimization of Case II, maximizing the overall output.

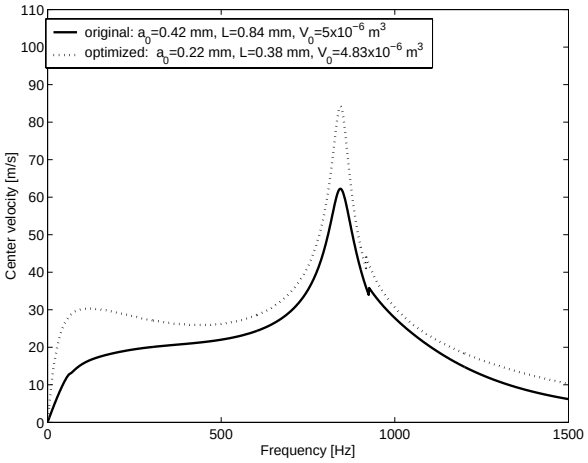

Figure 9: Optimization of Case II, maximizing the second peak.

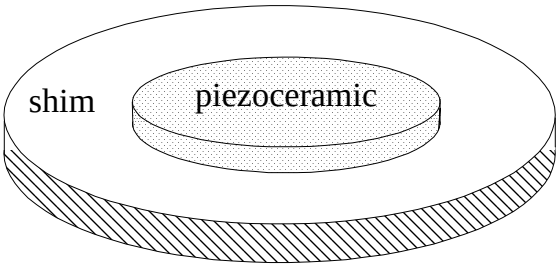

Figure 10: Top view of the inner-disc piezoelectric composite diaphragm configuration.

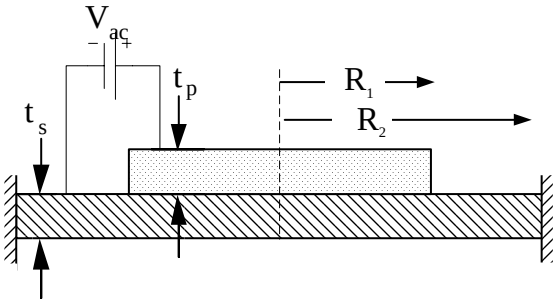

Figure 11: Cross-section of the inner-disc piezoelectric composite diaphragm configuration.

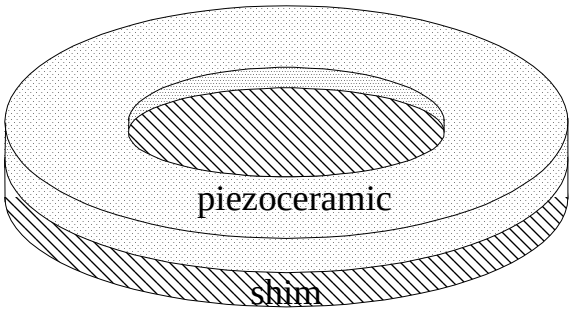

Figure 12: Top view of the outer-ring composite piezoelectric diaphragm configuration.

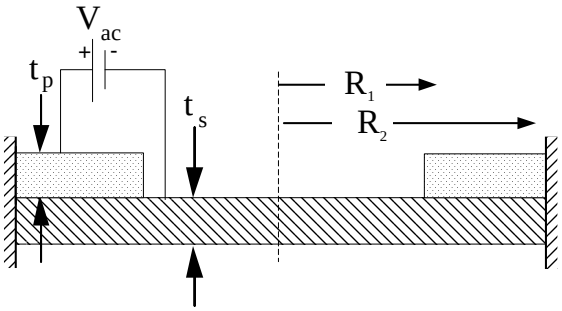

Figure 13: Cross-section of the outer-ring piezoelectric composite diaphragm configuration.